Rare Metal Materials and Engineering
Volume 48, Issue 4, April 2019
Available online at www.rmme.ac.cn

Science Press

Cite this article as: Rare Metal Materials and Engineering, 2019, 48(4): 1109-1115.

ARTICLE

Dynamic Globularization Kinetics and Finite Element Analysis for the Hot Working of Ti-5Al-5Mo-5V-3Cr-1Zr with Initial Lamellar Microstructure

Dai Yong, Lv Yaping, Li Shaojun, Zhang Xiaoyong, Zhou Kechao

State Key Laboratory of Powder Metallurgy, Central South University, Changsha 410083, China

Abstract: To predict the microstructure evolution of the Ti-55531 (Ti-5Al-5Mo-5V-3Cr-1Zr) with initial lamellar α, the dynamic globularization kinetics model of Ti-55531 during hot deformation was characterized by Avrami equation. A series of thermal simulation experiments were conducted to obtain the curves of stress σ versus strain ε to determine the equation parameters. By further transforming the stress-strain (σ-ε) curves into strain hardening rate dσ/dε-ε curve, the critical strain ε_c (corresponding to the minimum value of dσ/dε) and the peak strain ε_p (the strain at dσ/dε=0) were obtained. The dynamic globularized fraction f_g at different deformation conditions was also measured. Sequentially, the parameters in the Avrami equation were determined from the linear fitting of the relationships among strain rate, temperature, and dynamic globularized fraction. The as-obtained Avrami equation was expressed as $f_g=1-\exp[-0.5783((\varepsilon-\varepsilon_c)/\varepsilon_c)^{0.907}]$, where $\varepsilon_c=3.315\varepsilon_p$ and $\varepsilon_p=1.249\times10^{-4}\dot{\varepsilon}^{0.0807}\exp(58580/RT)$. Finally, the as-obtained dynamic globularization kinetic model was implanted into finite element program to simulate dynamic globularization kinetics. By combining the dynamic globularization kinetics model with the finite element method, the dynamic globularization of the lamellar α was predicted effectively.

Key words: near β titanium alloy; Ti-55531; hot deformation; dynamic globularization kinetics model; finite element method

Near β titanium alloys such as Ti-55531 (Ti-5Al-5Mo-5V-3Cr-1Zr) are expected to be applicable for thick section aerospace components due to their high specific strength, toughness and fatigue strength[1,2]. During the manufacturing of large structural components, thermomechanical processing is necessary not only for shaping but also for obtaining the required mechanical properties by controlling microstructure. The mechanical properties of titanium alloy mainly depend on the content, size, and distribution of the lamellar and equiaxed α phase[3-5]. Thermal deformation parameters, such as temperature, strain rate, and strain, have an important influence on the fragmentation/globularization of lamellar α into equiaxed morphology[5-7]. How to predict the dynamic globularization of lamellar α and deformation behavior of titanium alloy at different processing conditions has become a crucial issue.

Many experimental studies have been carried out on the dynamic globularization of two-phase Ti-alloys[8,9]. However, these experimental results can only be used to analyze the microstructural characteristic in a small area (for example, millimeter-scale in the scanning electron microscopic view), which cannot show the microstructural distribution in the whole component. With the development of computer technology, the reliability and accuracy of the finite element are greatly improved, making it become one of the most important and effective methods to analyze the large-scale regional microstructural distribution[10,11]. Kim et al[12] used three-dimensional crystal plasticity finite element method (CPFEM) to simulate microstructure and texture evolution during channel die compression of a body-centered cubic (bcc) polycrystalline material of interstitial free (IF) steel. Quan et al[13] studied the spatio-temporal phase transformation and

Received date: April 25, 2018
Foundation item: 2015 Independent Project of State Key Laboratory of Powder Metallurgy; Key Research and Development Plan of Hunan Province (2016JC2003)
Corresponding author: Zhang Xiaoyong, Ph. D., State Key Laboratory of Powder Metallurgy, Central South University, Changsha 410083, P. R. China, Tel: 0086-731-88836264, E-mail: zhangxiaoyong@csu.edu.cn

dynamic recrystallization (DRX) behaviors of Ti-6Al-4V. The finite element (FE) analysis shows the accurate simulation of the dynamic recrystallization. Therefore, the FEM has been quite promising in offering solutions to predict the microstructure evolution during hot deformation. But few investigations simulate the dynamic globularization of lamellar α in Ti-alloys.

Therefore, this paper focused on the dynamic globularization kinetics of near β Ti-alloy Ti-55531 using FEM. Firstly, the stress-strain curves were obtained by the thermal simulation tests. A quantitative statistical analysis and the characterization of microstructure evolution were adopted, and thus the dynamic globularization kinetics model was established. Furthermore, the dynamic globularization kinetics model was implanted into DEFORM-3D finite element program by developing FORTRAN codes, and then a series of simulations were conducted to obtain the evolution of the volume fraction of globular α phase at different deformation conditions. Finally, the simulation results were verified by experimental data.

1 Experiment

A Φ200 mm Ti-55531 forged bar (Hunan Goldsky Titanium Industry Technology Co. Ltd, China) was used as the starting material. Its alloy composition detected by PS-6 inductively coupled plasma was as follows in wt%: 5.4 Al, 4.9 Mo, 5.4 V, 3.16 Cr, 1.3 Zr, 0.12 Fe, 0.013 C, 0.0009 H, 0.07 O, 0.018 N with the balance Ti. And the β-transus temperature was approximately 825±5 °C measured by a metallographic method. To obtain the lamellar α microstructure, a 100 mm×60 mm×20 mm billet cut from the forged bar was solution heated at 880 °C for 15 min, water quenched, and then aged at 600 °C for 120 min, followed by a final water quenching. As shown in Fig.1, the acicular α with 2~4 μm in length and 0.2~0.5 μm in width are homogeneously distributed in the β matrix. And the triangle orientation relationship appears among acicular α. The volume fraction of α phase is about 30 vol% measured by photo pixels counting.

Several cylindrical specimens were linearly cut from the thermally-treated billet and then mechanically polished to Φ8 mm×12 mm. Isothermal compression was carried out on a Gleeble-3500 machine at 750~825 °C and strain rate of 10^{-3}~10^{0} s^{-1} in accordance with the ASTM: E209-00. A thermocouple with a diameter of 0.08 mm was welded at the mid-height side of the specimen to measure the temperature. The graphite foil and tantalum film were placed between the specimen and machine anvils for lubrication. The specimens were resistance-heated to the set temperature at the heating rate of 10 °C/s compressed to the true strain of 0.1~0.7, and then immediately cooled by an argon gas-jet to retain the deformed microstructure for the subsequent micro-observation. The measured load/displacement data were recorded and then transferred into the stress/strain data by testing machine automatically.

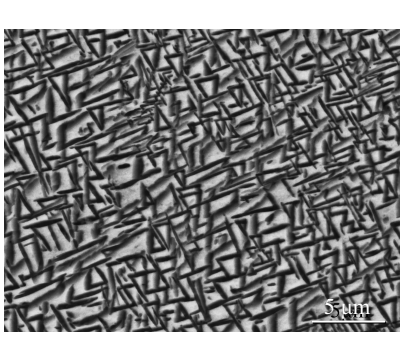

Fig.1 SEM micrograph of the heat-treated Ti-55531

The compressed specimens were cut along the cylinder axis line. The cutting faces were mechanically polished and then etched by 1.5 mL HF+3 mL HNO_3+100 mL H_2O. The microstructure at the center of specimens was observed by a scanning electron microscope (SEM, NOVATM Nano SEM 230). Globularization behavior of the α lamellae was then quantified using SEM photographs with a quantitative metallographic image analysis system (Image-pro plus 6.0) considering α phase with the aspect ratio (length/width) lower than 2 as a globular[14,15].

2 Results and Discussion

2.1 Flow behavior and microstructure evolution

True stress-true strain curves obtained at the temperature of 750~825 °C and strain rates of 10^{-3}~10^{0} s^{-1} are shown in Fig.2. During hot deformation, the flow stress increases to a peak at a low strain and then decreases continuously with straining under the competition between working hardening and flow softening. The degree of work hardening is closely related to the deformation temperature[16]. The increasing of deformation temperature results in the increasing of atomic average kinetic energy and then the decreasing of critical resolved shear stress. Also, α phase with the hcp structure is partly transformed into the β phase with the bcc structure. And the softening such as dynamic recovery and dynamic recrystallization is easier. Thereby the flow stress is reduced. Meanwhile, the stress increases with the increasing of strain rate, because the deformation time is not enough for the dislocation annihilation and microstructure evolution at higher strain rate[17].

Fig.3 shows the deformed microstructures of Ti-55531 at different conditions. Apparently, at 750 °C, strain rate of 10^{-1} s^{-1} and small true strain of 0.2, the α particles are still similar to those in the initial microstructure, and only a small amount of lamellar α breaks up. While at true strain of 0.6, microstructure changes significantly, in which a large amount of globularized α phase can be observed. Globularization of lamellar α is positively correlated with true strain. It is observed that the break-up or globularization of lamellar α increases with the decrease of strain rate, especially at the high true strain. For example, after compressing to the true strain of 0.4 at 750 °C, only a small amount of lamellar α break up at

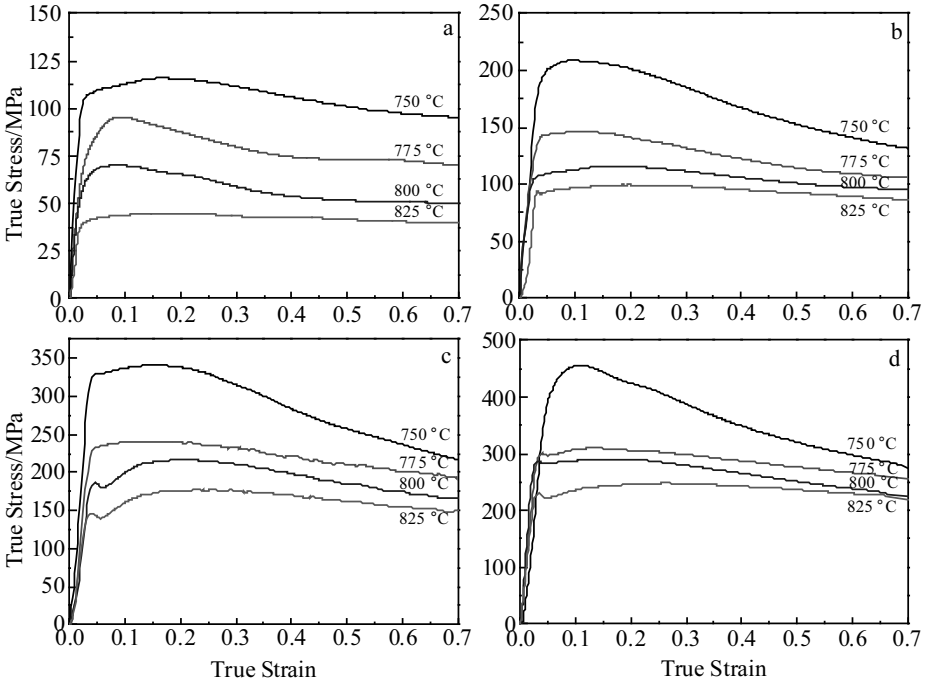

Fig.2 True stress-strain curves of Ti-55531 under different deformation conditions: (a) 10^{-3} s^{-1}, (b) 10^{-2} s^{-1}, (c) 10^{-1} s^{-1}, and (d) 10^{0} s^{-1}

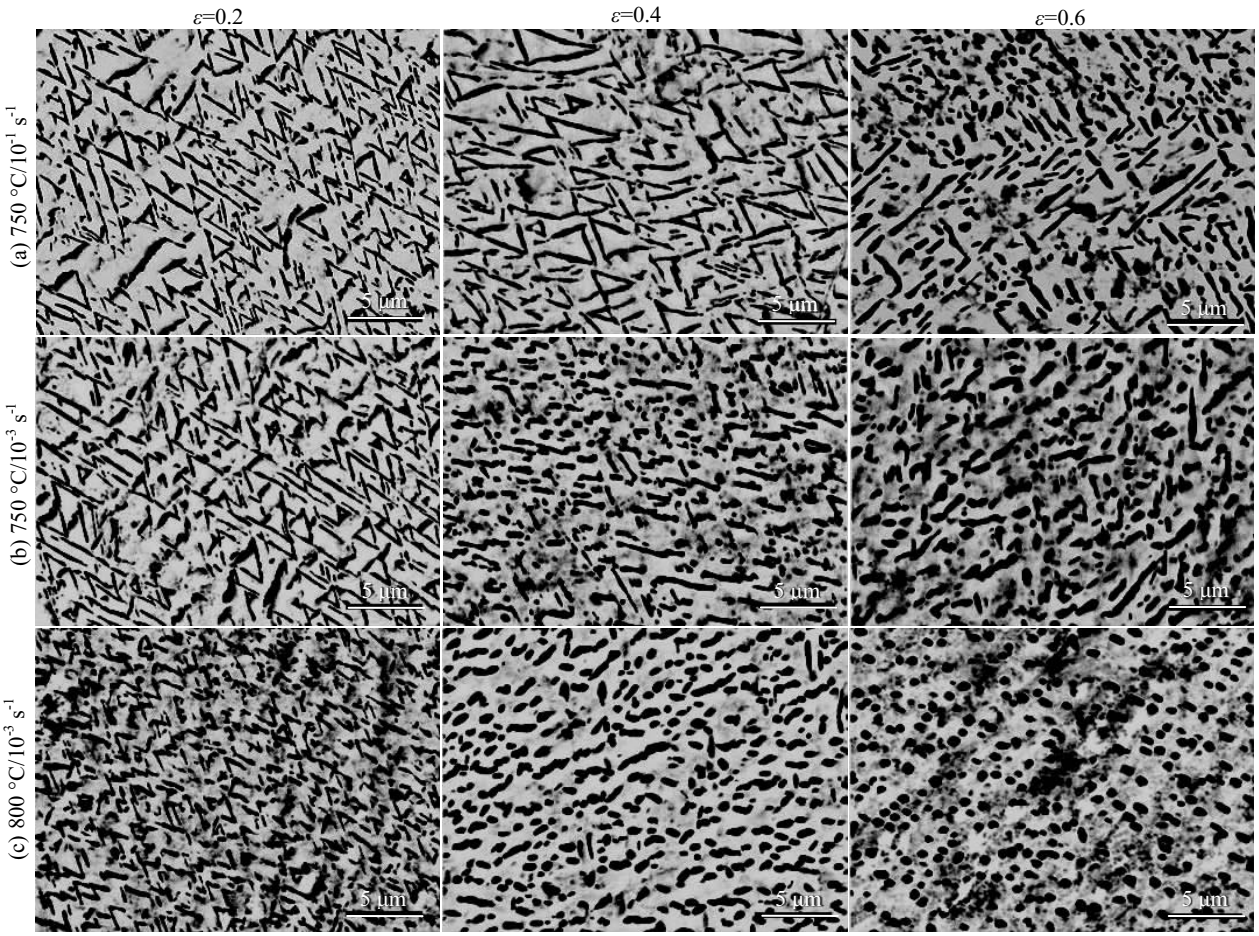

Fig.3 Microstructures of acicular α at different deformation conditions

the strain rate of 10^{-1} s^{-1} (Fig.3a), while the remarkable fragmentation of lamellar α are observed at the strain rate of 10^{-3} s^{-1} (Fig.3b). Meanwhile, with the increasing of temperature from 750 °C to 800 °C (Fig.3c), the globularization fraction of lamellar α is obviously accelerated. A large amount of lamellar α are broken even at the low true strain of 0.2, and then fragmented and globularized completely at the true strain of 0.6.

Using Image-pro plus 6.0, the dynamic globularized fraction at different deformation conditions was quantitatively measured, as summarized in Table 1.

Table 1 Globularization fraction at different hot deformation conditions

Temperature/ °C	Strain rate/s^{-1}	True strain					
		0.2	0.3	0.4	0.5	0.6	0.7
750	10^{-1}	0.011	0.034	0.101	0.255	0.391	0.455
	10^{-2}	0.028	0.048	0.201	0.331	0.459	0.511
	10^{-3}	0.037	0.154	0.285	0.458	0.588	0.627
775	10^{-1}	0.036	0.076	0.153	0.353	0.489	0.539
	10^{-2}	0.048	0.098	0.222	0.414	0.589	0.636
	10^{-3}	0.090	0.246	0.383	0.569	0.632	0.768
800	10^{-1}	0.041	0.100	0.227	0.451	0.566	0.650
	10^{-2}	0.052	0.215	0.386	0.560	0.636	0.724
	10^{-3}	0.130	0.320	0.497	0.640	0.736	0.803

2.2 Dynamic globularization kinetics model

As shown in Fig.3, the globularization fraction is very sensitive to the deformation conditions. The similar characteristics have been observed on Ti-6Al-4V, which can be described by an Avrami type equation[18].

$$f_g = 1 - \exp[-k((\varepsilon - \varepsilon_c)/\varepsilon_c)^n] \quad (1)$$

where, f_g is the volume fraction of dynamic globularized α, ε_c is the critical strain for initiation of dynamic globularization, and n and k are the material constants.

2.2.1 Critical strain and peak strain

Existing researches show that during the process of hot deformation, the microstructure evolution characteristics will be reflected on the macroscopic stress-strain curve[19-22]. At the beginning of the deformation, true stress (σ) increases rapidly to the peak value. With the further increasing of true strain (ε), the flow stress decreases gradually, showing the continuous softening up to steady flow. The flow softening is resulted from the rotation, plastic bending, breaking up and globularization of lamellar α[23]. Before the inflection point (corresponding to the minimum value of $d\sigma/d\varepsilon$), the rotation and plastic bending of lamellar α play a dominant role in the flow softening. After the inflection point, the main action comes from the breaking up and globularization of lamellar α[24]. Therefore, the critical strain (ε_c) in Eq. (1) is the minimum value (namely at the inflection point) in the $d\sigma/d\varepsilon$-ε curve.

$$\varepsilon_c = a_1 \varepsilon_p \quad (2)$$

Additionally, the peak strain (ε_p) is the strain at $d\sigma/d\varepsilon$=0. The value of critical strain (ε_c) and peak strain (ε_p) at different thermal deformation conditions are listed in Table 2, and then plotted as the linear relationship in Fig.4, where the slope after linearly fitting is the value of a_1, namely 3.315.

Table 2 Values of critical strain (ε_c) and peak strain (ε_p) at different conditions

Characteristic strain	Strain rate/s^{-1}	Temperature/°C			
		750	775	800	825
ε_c	10^{-3}	0.250	0.200	0.180	0.130
	10^{-2}	0.280	0.240	0.200	0.180
	10^{-1}	0.350	0.300	0.260	0.240
	1	0.430	0.410	0.350	0.320
ε_p	10^{-3}	0.125	0.112	0.095	0.080
	10^{-2}	0.112	0.090	0.077	0.064
	10^{-1}	0.102	0.082	0.068	0.055
	1	0.090	0.068	0.051	0.038

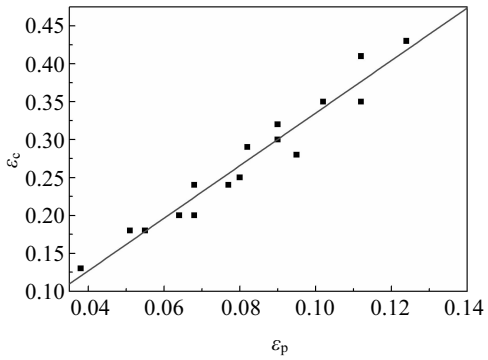

Fig.4 Relationship between critical strain (ε_c) and peak strain (ε_p)

2.2.2 Material constant a_2, m and deformation activation energy Q

According to Semiatin[25] and Sellars[26] et al, the critical strain (ε_c) and peak strain (ε_p) are the functions of deformation temperature and strain rate. The relationship among peak strain, strain rate, and temperature can be characterized by Sellars model:

$$\varepsilon_p = a_2 \dot{\varepsilon}^m \exp(Q/RT) \quad (3)$$

where, ε_p is the peak strain, Q is the thermal deformation activation energy, R is the gas constant, T is the absolute temperature, and a_2 and m are the material constants.

The expressions of the critical strain (ε_c) for the breaking up of α are obtained by taking Eq. (2) into Eq. (3):

$$\varepsilon_c = a_1 a_2 \dot{\varepsilon}^m \exp(Q/RT) \quad (4)$$

By taking natural logarithm and then partial derivative on both sides of Eq. (4), the deformation activation energy Q can be expressed as:

$$\ln \varepsilon_c = (Q/R) \cdot (1/T) + m \ln \dot{\varepsilon} + \ln(a_1 a_2) \quad (5)$$

The relationships between $\ln\varepsilon_c$ and $1/T$ at different strain rates are fitted linearly as shown in Fig.5, in which the slope of fitted line is the value of Q/R. Fig.5 shows that the fitted lines have the similar slope. By averaging three slope values, Q/R was obtained as 7045.97. It can be calculated as Q=58 580 J·mol^{-1}.

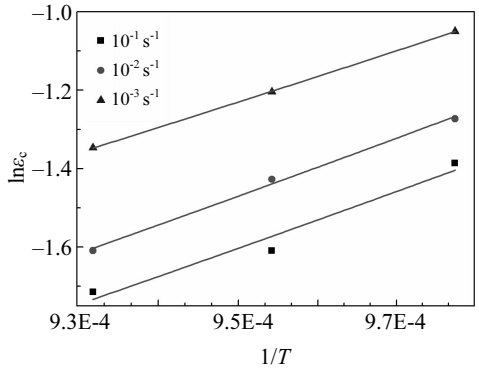

Fig.5 Linear fitting between $\ln\varepsilon_c$ and $1/T$

Also, the material constant m can be expressed as:

$$\ln\varepsilon_c = m\ln\dot{\varepsilon} + Q/RT + \ln(a_1a_2) \quad (6)$$

The relationships between $\ln\varepsilon_c$ and $\ln\dot{\varepsilon}$ at different strain rates are fitted linearly as shown in Fig.6. m is the mean value of three slope values, and here it is 0.0803. By substituting a_1, Q, and m into Eq. (6), 9 values of material constant a_2 are obtained, and then the mean value of a_2 is 1.29×10^{-4}.

2.2.3 Material constant k, n

By taking natural logarithm and then partial derivative on both sides of Eq. (1), the material constants n and k can be expressed as:

$$\ln[\ln(1/(1-f_g))] = \ln k + n\ln((\varepsilon-\varepsilon_c)/\varepsilon_c) \quad (7)$$

Fig.7 shows the $\ln[\ln(1/(1-f_g))]$-$\ln[(\varepsilon-\varepsilon_c)/\varepsilon_c]$ curve obtained by fitting into the experimental data. It can be seen from Fig.8 that $\ln[(\varepsilon-\varepsilon_c)/\varepsilon_c]$ and $\ln[\ln(1/(1-f_g))]$ satisfy the linear relationship.

Parameter values are obtained by linear regression processing, as follows: n=0.907, k=0.5783 (correlation coefficient R^2=0.83). Finally, the as-obtained dynamic globularization kinetic model is described as:

$$\begin{cases} f_g = 1-\exp[-0.5783((\varepsilon-\varepsilon_c)/\varepsilon_c)^{0.907}] \\ \varepsilon_c = 3.315\varepsilon_p \\ \varepsilon_p = 1.249\times10^{-4}\dot{\varepsilon}^{0.0807}\exp(58580/RT) \end{cases} \quad (8)$$

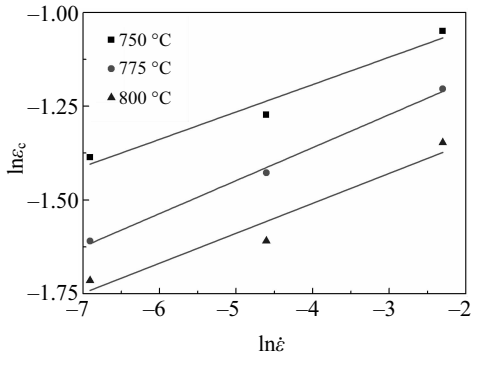

Fig.6 Linear fitting between $\ln\varepsilon_c$ and $\ln\dot{\varepsilon}$

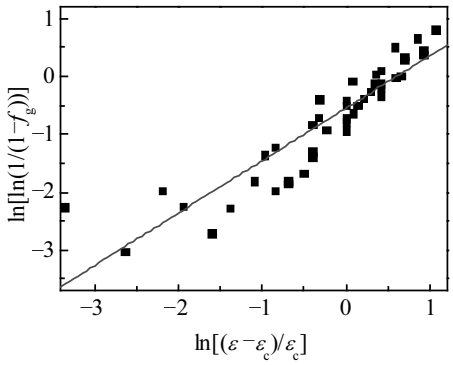

Fig.7 Relationship between globularization fraction of lamellar α and true strain

Fig.8 shows the good agreement between the dynamic globularization kinetics model data and experimental data.

2.3 Simulation of dynamic globularization kinetics and experimental verification

Eq. (8) representing the α globularization kinetic model of Ti-55531 was implanted into DEFORM using FORTRAN compile to simulate the hot compression of cylinder workpiece. During the finite element simulation, the friction between workpiece and anvil was set as shearing with the friction coefficient of 0.3, the heat transfer coefficient was set to 11 $N\cdot s^{-1}\cdot mm^{-1}\cdot{}^{o}C^{-1}$, and the boundary conditions were consistent with the experimental details. In addition, the workpiece was set as a plastic body, while the anvil was set as a rigid body. The total number of nodes and elements were 16 307 and 70 824, respectively.

Fig.9 and 10 show the effects of temperature (at 10^{-2} s^{-1}) and strain rate (at 750 °C) on the globularization fraction distribution after hot compressing to the true strain of 0.7. It can be obviously found that the distribution of globularization fraction is inhomogeneous at every deformation condition. The maximum and minimum globularization fraction values locate at the center region of cylindrical body (P_1) and of end surface, respectively. With the increasing of temperature at strain rate of 10^{-2} s^{-1} and decreasing of strain rate at 750 °C, P_1 region (maximum globularization fraction) enlarges, which suggests the increasing of average globularization fraction, namely the acceleration of dynamic globularization kinetics.

To verify the above simulation results, Fig.11 show the microstructures at the center of thermal simulation specimens compressed to the true strain of 0.7, which are corresponding to the P_1, P_2 and P_3 regions in Fig.9 and 10. The dynamic globularized fractions of 0.505, 0.738 and 0.619 at the P_1, P_2 and P_3 regions of FEM results are consistent with those in Fig.11a, 11b, and 11c as listed in Table 1. Therefore, the simulation results show the high accuracy. And through FEM simulation, the dynamic globularization at a different region of specimens during hot deformation can be described numerically.

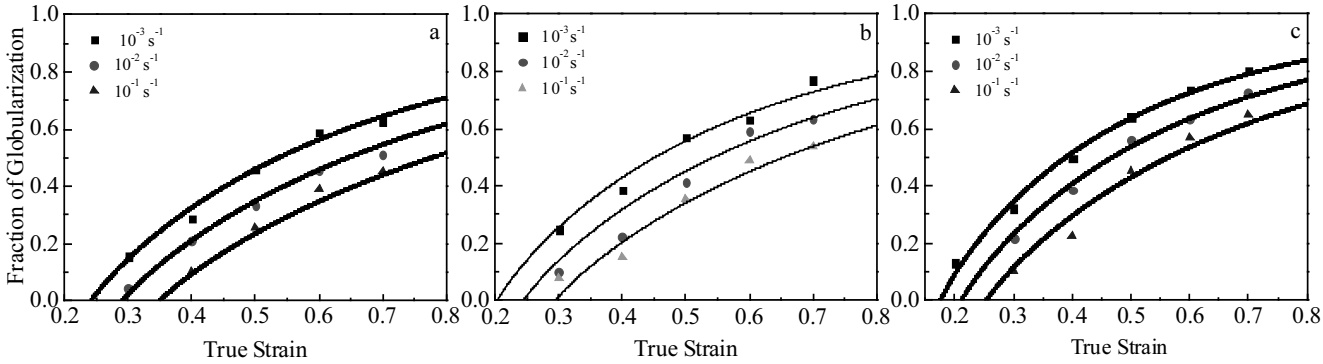

Fig.8 Comparison of globularization kinetic model with experimental data: (a) 750 °C, (b) 775 °C, and (c) 800 °C

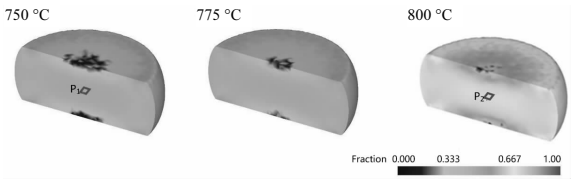

Fig.9 Globularization fraction of Ti-55531 cylinder deformed at the strain rate of 10^{-2} s^{-1} and different temperatures to the strain of 0.7

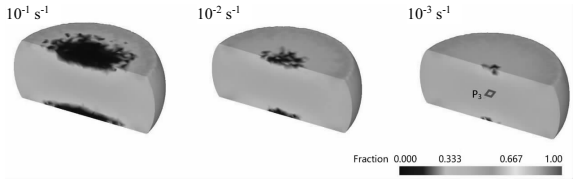

Fig.10 Globularization fraction of Ti-55531 cylinder deformed at 750 °C and different strain rates to the strain of 0.7

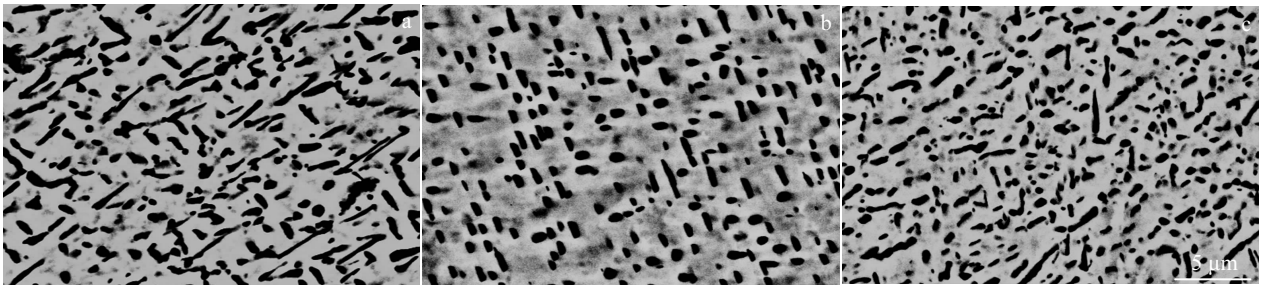

Fig.11 Microstructures at the center region of cylindrical body deformed at different deformation conditions to the strain of 0.7: (a) 750 °C/10^{-2} s^{-1}, (b) 800 °C/10^{-2} s^{-1}, and (c) 750 °C/10^{-3} s^{-1}

3 Conclusions

1) Deformation parameters have an effect on dynamic globularization of the lamellar α. At the same strain rate, the dynamic globularized fraction increases with increasing deformation temperature. At the same deformation temperature, the dynamic globularized fraction increases with decreasing strain rate.

2) Combined with stress-strain curves and microstructure evolution, the dynamic globularization kinetics model of lamellar α based on Avrami equation is constructed. The as-obtained dynamic globularization kinetic model is described as:

$$\begin{cases} f_g = 1 - \exp[-0.5783((\varepsilon - \varepsilon_c)/\varepsilon_c)^{0.907}] \\ \varepsilon_c = 3.315\varepsilon_p \\ \varepsilon_p = 1.249 \times 10^{-4} \dot{\varepsilon}^{0.0807} \exp(58580/RT) \end{cases}$$

3) The Avrami equation has been implanted into the FEM program to simulate the dynamic globularization kinetics. The finite element simulation results show the inhomogeneity of dynamic globularization of α phase distribution. The maximum and minimum dynamic globularized fractions distribution regions locate at the center region of cylindrical body and of end surface, respectively. And the dynamic globularization distribution at different deformation parameters has been described accurately.

References

1 Warchomicka F, Poletti C, Stockinger M. *Materials Science and Engineering A*[J], 2011, 528(28): 8277

2 Dikovits M, Poletti C, Warchomicka F. *Metallurgical and Materials Transactions A*[J], 2014, 45(3): 1586

3 Karpat Y. *Journal of Materials Processing Technology*[J], 2011,

211(4): 737
4 Welsch G, Boyer R, Collings E W. *Materials Properties Handbook: Titanium Alloys*[M]. OH: ASM International, 1993
5 Stefansson N, Semiatin S L. *Metallurgical and Materials Transactions A*[J], 2003, 34(3): 691
6 Fan J K, Kou H C, Lai M J *et al*. *Materials & Design*[J], 2013, 49: 945
7 Ning Y Q, Xie B C, Liang H Q *et al*. *Materials & Design*[J], 2015, 71: 68
8 Furuhara T, Poorganji B, Abe H *et al*. *JOM*[J], 2007, 59(1): 64
9 Chen H Q, Cao C X. *Rare Metal Materials and Engineering*[J], 2011, 40(6): 946
10 Li H W, Sun X X, Yang H. *International Journal of Plasticity*[J], 2016, 87: 154
11 Knezevic M, Drach B, Ardeljan M *et al*. *Computer Methods in Applied Mechanics and Engineering*[J], 2014, 277: 239
12 Kim D K, Kim J M, Park W W *et al*. *Computational Materials Science*[J], 2015, 100: 52
13 Quan G Z, Pan J, Zhang Z H. *Materials & Design*[J], 2016, 94: 523
14 Yang L, Wang B Y, Liu G *et al*. *Materials & Design*[J], 2015, 85: 135
15 Wang K X, Zeng W D, Zhao Y Q *et al*. *Materials Science and Engineering A*[J], 2010, 527(10-11): 2559
16 Sun Y, Zeng W D, Zhao Y Q *et al*. *Computational Materials Science*[J], 2010, 48(3): 686
17 Follansbee P S, Gray G T. *Metallurgical and Materials Transactions A*[J], 1989, 20(5): 863
18 Jia J B, Zhang K F, Lu Z. *Journal of Alloys and Compounds*[J], 2014, 617: 429
19 Song H W, Zhang S H, Cheng M. *Journal of Alloys and Compounds*[J], 2009, 480(2): 922
20 Semiatin S L, Thomas J F, Dadras P. *Metallurgical Transactions A*[J], 1983, 14(11): 2363
21 Ma X, Zeng W D, Tian F *et al*. *Materials Science and Engineering A*[J], 2012, 548: 6
22 Li C, Zhang X Y, Li Z Y *et al*. *Materials Science and Engineering A*[J], 2013, 573: 75
23 Jones N G, Jackson M. *Materials Science and Technology*[J], 2011, 27(6): 1025
24 Xu J W, Zeng W D, Jia Z Q *et al*. *Journal of Alloys and Compounds*[J], 2014, 603: 239
25 Semiatin S L, Seetharaman V, Weiss I. *Materials Science and Engineering A*[J], 1999, 263(2): 257
26 Sellars C M. *Materials Science and Technology*[J], 1990, 6(11): 1072

针片 Ti-5Al-5Mo-5V-3Cr-1Zr 热加工过程中的球化动力学及有限元仿真

戴　勇，吕亚平，李少君，张晓泳，周科朝
(中南大学 粉末冶金国家重点实验室，湖南 长沙 410083)

摘　要：为了预测初始层状 α 的 Ti-55531（Ti-5Al-5Mo-5V-3Cr-1Zr）的微观组织演变，采用 Avrami 方程对 Ti-55531 热变形过程中的动态球化动力学模型进行了表征。为了确定方程的参数，为了获得应力-应变 (σ-ε) 曲线进行了一系列热模拟实验。通过进一步将 σ-ε 曲线转化为应变硬化速率 $\mathrm{d}\sigma/\mathrm{d}\varepsilon$-$\varepsilon$ 曲线，可以获得临界应变 ε_c（对应 $\mathrm{d}\sigma/\mathrm{d}\varepsilon$ 的最小值）和峰值应变 ε_p（$\mathrm{d}\sigma/\mathrm{d}\varepsilon$=0 时的应变）。还测量了不同变形条件下的动态球化分数 f_g。接下来，通过线性拟合应变率，温度和动态球化部分之间的关系来确定 Avrami 方程中的参数。得到的 Avrami 方程表示为 $f_g=1-\exp[-0.5783((\varepsilon-\varepsilon_c)/\varepsilon_c)^{0.907}]$，其中 $\varepsilon_c=3.315\varepsilon_p$，$\varepsilon_p=1.249\times10^{-4}\dot{\varepsilon}^{0.0807}\exp(58580/RT)$。最后，将获得的动态球化动力学模型植入有限元程序中模拟动态球化动力学。将动态球化动力学模型与有限元方法相结合，有效地预测了针片 α 动态球化动力学过程。

关键词：近 β 钛合金；Ti-55531；热变形；球化动力学模型；有限元仿真

作者简介：戴　勇，男，1992 年生，硕士，中南大学粉末冶金国家重点实验室，湖南 长沙 410083，E-mail: dycsu2011@126.com